HAL
archives-ouvertes.fr

Analytically-Based Simulation for Corrosion Detection by Guided Waves

Evgeny Glushkov, Natalia Glushkova, Artem Eremin, Victor Giurgiutiu

▶ **To cite this version:**

Evgeny Glushkov, Natalia Glushkova, Artem Eremin, Victor Giurgiutiu. Analytically-Based Simulation for Corrosion Detection by Guided Waves. Le Cam, Vincent and Mevel, Laurent and Schoefs, Franck. EWSHM - 7th European Workshop on Structural Health Monitoring, Jul 2014, Nantes, France. 2014. <hal-01020319>

HAL Id: hal-01020319
https://hal.inria.fr/hal-01020319

Submitted on 8 Jul 2014

HAL is a multi-disciplinary open access archive for the deposit and dissemination of scientific research documents, whether they are published or not. The documents may come from teaching and research institutions in France or abroad, or from public or private research centers.

L'archive ouverte pluridisciplinaire **HAL**, est destinée au dépôt et à la diffusion de documents scientifiques de niveau recherche, publiés ou non, émanant des établissements d'enseignement et de recherche français ou étrangers, des laboratoires publics ou privés.

7th European Workshop on Structural Health Monitoring
July 8-11, 2014. La Cité, Nantes, France

ANALYTICALLY-BASED SIMULATION FOR CORROSION DETECTION BY GUIDED WAVES

Evgeny Glushkov[1], **Natalia Glushkova**[1], **Artem Eremin** [1], **Victor Giurgiutiu** [2]

[1] *Kuban State University, Institute for Mathematics, Mechanics and Informatics, 149 Stavropolskaya st., 350040 Krasnodar, Russia*
[2] *University of South Carolina, Department of Mechanical Engineering, 315 Main Street, 29208 Columbia, SC, USA*

evg@math.kubsu.ru

ABSTRACT

To create a theoretical basis for guided wave detection and identification of corrosion damages, a set of analytically based computer models of various complexity has been developed. The present paper is focused on the simplest and fastest beam model for stepped and notched waveguides, which has exhibited a wide frequency range of reasonable coincidence with the results obtained within more complex integral equation based model for a 2D notched elastic strip.

KEYWORDS : *guided waves, diffraction, corrosion detection, layer and beam models*

INTRODUCTION

Guided wave (GW) detection and identification of corrosion damages is still a challenging task for SHM [1]. Corrosion areas are less contrast than "conventional" cracks, delaminations and disbondings which give strongly localized response. Therefore, the extraction of corrosion indications from received signals (both scattered by and getting through the corrosion area) requires more comprehensive processing based on fast computer simulation of GW diffraction by surface irregularities. Commercial FEM packages are rather time-consuming, especially with 3D scattering, so it is worthy to select as simple models as possible, which, nevertheless, capture the characteristic diffraction features of areas affected by corrosion.

Motivated by that idea, we have developed a hierarchy of 2D and 3D semi-analytical models of varying complexity, comparing them with each other, with benchmark results of other authors and with experimental measurements, estimating in this way the range of applicability of each model. In descending order of complexity there are

1) laminate element method (LEM) for 3D scattering by depressions and cavities [2] ;
2) LEM based models for GW diffraction by arbitrarily shaped notches in 2D elastic strip waveguides;
3) expansion in series in propagating and evanescent normal modes for 2D stepped waveguides [3];
4) eccentrically butted beams of different thickness as 1D stepped and notched waveguides.

The closest analogue of the first LEM based model is the approach developed by Moreau et al [4]. Numerical comparisons with the GW scattering diagrams obtained by that method exhibit a full coincidence. The second and third 2D models have been tested against the numerical and experimental results by Lowe et al [5] as well as by checking the boundary conditions at the joint line and the energy balance among the incident, reflected, transmitted and converted modes. In turn, these models were used to estimate the range of applicability of the simplest and fastest beam models. The latter has demonstrated an unexpectedly wide frequency range in which the reflection and transmission coefficients reasonably coincide with those for the fundamental S_0 and A_0 modes in 2D stepped and notched waveguides.

Copyright © Inria (2014)

The present paper is focused on this beam model: first, a mathematical model for GW propagation in pristine and damaged Euler-Bernoulli beams is given and quantitative energy characteristics of corresponding waves are introduced. After that a corresponding 2D LEM based approach for a notched plate is briefly described to verify the applicability limits of the simplified model. Finally the results obtained by the both approaches are compared and discussed.

1. BEAM MODEL

An elastic beam of width b and thickness h occupies the volume $|x| < \infty$, $|y| \le b/2$ and $|z| \le h/2$ in the Cartesian coordinate system. Its deformation is independent of y, so it is specified by the independent of y displacement vector $\mathbf{u} = (u_x, 0, u_z)$ lying in the central plane (x,z) (2D plane-strain deformation, Fig. 1a).

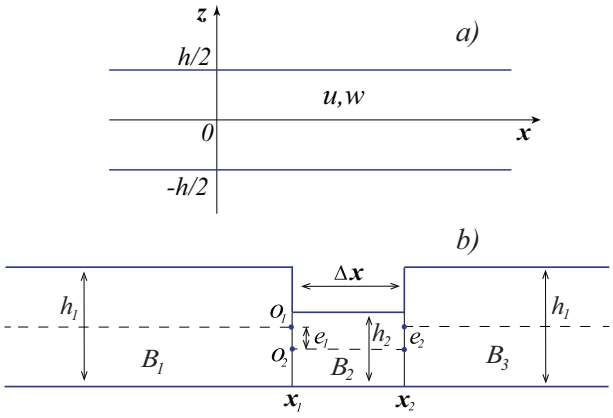

Figure 1 : Geometry of problem: pristine beam (top) and notched waveguide (bottom).

Within the beam assumptions

$$u_x(x,z) = u(x) - zw'(x) \tag{1}$$

$$u_z(x,z) = w(x), \tag{2}$$

where $u(x)$ and $w(x)$ are 1D functions set on the beam axis $-\infty < x < \infty$, $y = 0$, $z = 0$. With a steady-state time-harmonic oscillation $\mathbf{u}e^{-i\omega t}$, the vector $\mathbf{u}$ is a complex vector of displacement amplitude, and the functions $u(x)$ and $w(x)$ obey the beam equations

$$u'' + \zeta_1^2 u = 0 \tag{3}$$

$$w^{IV} - \zeta_2^4 w = 0. \tag{4}$$

Here $\zeta_1^2 = \frac{\rho}{Y}\omega^2$ and $\zeta_2^4 = \frac{\rho A}{YI}\omega^2 = \frac{12\rho}{Yh^2}\omega^2$, Y is the modulus of elasticity (Young modulus), ρ is density, $A = bh$ is the area of beam's cross-section, $I = \iint\limits_A z^2 dydz = bh^3/12$ is the moment of inertia, $\omega = 2\pi f$ is angular frequency, f is frequency.

The beam supports longitudinal and flexural guided waves S_0 and A_0, which are specified by the eigensolutions of Eqs. (3) and (4), respectively:

$$S_0: \quad u_0(x) = S_0 e^{i\zeta_1 x} \tag{5}$$

$$A_0: \quad w_0(x) = A_0 e^{i\zeta_2 x} \tag{6}$$

The amplitudes S_0 and A_0 are arbitrary complex constants, ζ_1 and ζ_2 are the wavenumbers of these waves. Besides, the evanescent terms $Be^{\pm\zeta_2 x}$ also satisfy Eq. (4).

Force resultants, e.g., longitudinal force N, moment M and shear force V are expressed in terms of the displacement components:

$$N(x) = \iint\limits_A \sigma_x dydz = YAu'(x), \;\; M(x) = \iint\limits_A z\sigma_x dydz = -YIw''(x) \tag{7}$$

$$V(x) = M'(x) = -YIw'''(x). \tag{8}$$

Here $\sigma_x(x) = Y\varepsilon_x = Y(u' - zw'')$ is cross-sectional traction. The corresponding shear stress τ_{xz} is estimated via the assumption of even distribution of the force V over the cross-section A:

$$\tau_{xz}(x) = V/A = -Y\frac{I}{A}w'''(x). \tag{9}$$

2. WAVE ENERGY

In a time-harmonic wave field, the energy flux is estimated in terms of quantities averaged over the period of oscillation $T = 2\pi/\omega = 1/f$. The averaged density and the direction of energy flux passing through a spatial point $\mathbf{x}$ per unit time is specified by the energy density vector $\mathbf{e}(\mathbf{x}) = (e_x, e_y, e_z)$. The total amount of energy E, carried by harmonic waves through a certain surface S per unit time (in fact, the power of the energy flux), is determined via the integration of the energy density over S:

$$E = \iint\limits_S e_n(\mathbf{x}) dS. \tag{10}$$

Here $e_n = (\mathbf{e}, \mathbf{n}) = \frac{\omega}{2}\mathrm{Im}(\tau_n, \mathbf{u})$ is the normal to S component of vector $\mathbf{e}$; $\mathbf{n}(\mathbf{x})$ is the unit surface normal at the current point $\mathbf{x} \in S$; τ_n is the stress vector at a surface element specified by $\mathbf{n}$; the scalar product of complex vectors assumes the complex conjugation of the second factor hereinafter denoted with asterisk: $(\mathbf{a}, \mathbf{b}) = \sum\limits_i a_i b_i^*$.

For the calculation of wave energy carried by S_0 and A_0 guided waves along the beam, one has to take its cross-section A as the surface S in Eq. (10). At that, the normal $\mathbf{n} = (1,0,0)$, $\tau_x = (\sigma_x, 0, \tau_{xz})$, and E can be obtained as follows

$$\begin{aligned} E(x) &= b \int\limits_{|z|<h/2} e_x(x,z)dz = \tfrac{\omega}{2} bY\,\mathrm{Im} \int\limits_{|z|<h/2} [u'u^* + z^2 w''(w')^* - \tfrac{I}{A} w'''w^*]dz = \\ &= \tfrac{\omega}{2} Y\,\mathrm{Im}\,[Au'u^* + Iw''(w')^* - Iw'''w^*]. \end{aligned} \tag{11}$$

In view of the energy conservation law, $E(x)$ must be constant in the segments of ideally elastic waveguides free from wave sources and energy drains irrespective of their thickness variation.

For travelling waves (5) - (6)

$$u_0' u_0^* = i\zeta_1 |S_0|^2 \quad \text{and} \quad w_0''(w_0')^* = -w_0''' w_0^* = i\zeta_2^3 |A_0|^2,$$

thus,

$$E = E_S + E_A = \frac{\omega}{2} YA\zeta_1 |S_0|^2 + \omega YI\zeta_2^3 |A_0|^2. \tag{12}$$

The parts E_S and E_A are energy of S_0 and A_0 modes, respectively. They independently contribute into the the total amount of wave energy E transferred through the cross-section $x = \mathrm{const}$ per time unit.

Remark 1. In the case of waves propagating in opposite directions, they contribute into E with opposite signs:

$$E_S = \frac{\omega}{2} YA\zeta_1 (|S^+|^2 - |S^-|^2) \quad \text{and} \quad E_A = \omega YI\zeta_2^2 (|A^+|^2 - |A^-|^2)$$

for $u = S^+e^{i\zeta_1 x} + S^-e^{-i\zeta_1 x}$ and $w = A^+e^{i\zeta_2 x} + A^-e^{-i\zeta_2 x}$. Note that mixed terms such as $S^+(S^-)^*e^{2i\zeta_1 x}$ appear as complex conjugate pairs. Their sums, being complex conjugate values, do not affect the amount of energy E calculated via Eq. (11).

Remark 2. The evanescent terms also do not affect the amount of energy carried by GWs. For example, with $w = Ae^{i\zeta_2 x} + Be^{-\zeta_2}$, the mixed terms in $w''(w')^* - w'''w^*$ in Eq. (11) are real values of form $2\zeta_2^3[\mathrm{Im}\,(iAB^*e^{i\zeta_2 x}) - \mathrm{Re}\,(A^*Be^{-i\zeta_2 x})]e^{-\zeta_2 x}$.

3. BOUNDARY CONDITIONS IN THE DOCKING AREA

Let us consider a beam with a rectangular notch of length Δx and depth Δz. It may be treated as a joint of three beams B_1, B_2 and B_3 of, generally speaking, three different thicknesses h_1, h_2 and h_3. In the case under consideration $h_3 = h_1$, $\Delta x = x_2 - x_1$, $\Delta z = h_1 - h_2$, and the value $e = \Delta z/2$ is called "the eccentricity" of the non-coaxial beam B_2 (Fig. 1b). The central axis of the latter goes through the point $O_2(x_1, -e)$ in the global coordinate system (x, z). Therefore, the displacements in B_2 should be written in the local coordinates (x, y, z_2), where $z_2 = z + e$:

$$\begin{aligned} u_{x,2} &= u_2 - z_2 w_2' \\ u_{z,2} &= w_2 \end{aligned} \tag{13}$$

In these coordinates the moment and shear force are

$$\hat{M}_2(x) = \iint\limits_{A_2} z_2 \sigma_{x,2} dy dz_2 = -YI_2 w_2'' \quad \text{and} \quad V_2(x) = \hat{M}_2'(x) = -YI_2 w_2'''. \tag{14}$$

It is necessary to consider that $\hat{M}_2$ is calculated with respect to the local center O_2, while the calculation of the moment M_2 with respect to the same as in B_1 center O_1 leads to the additional, proportional to the eccentricity e, term:

$$M_2(x) = \iint\limits_{A_2} (z_2 - e)\sigma_{x,2} dy dz_2 = \hat{M}_2 - eN_2, \quad N_2 = YA_2 u_2'(x). \tag{15}$$

Note that the force V_2 is independent of coordinate system, it remains of form (14).

To formulate proper boundary conditions at the joining points x_1 and x_2, one should equate the displacements, forces and moments at these points. The displacement equality at $x = x_1$ entails three equalities connecting u_1 and w_1 with u_2 and w_2:

$$\begin{aligned} u_1 &= u_2 - ew_2' \\ w_1 &= w_2 \\ w_1' &= w_2' \end{aligned} \quad , \quad x = x_1, \tag{16}$$

while the force and moment equalities $N_1 = N_2$, $V_1 = V_2$, and $M_1 = M_2$ at $x = x_1$ yield more three links:

$$\begin{aligned} h_1 u_1' &= h_2 u_2' \\ h_1^3 w_1'' &= h_2^3 w_2'' + 12eh_2 u_2' \\ h_1^3 w_1''' &= h_2^3 w_2''' \end{aligned} \quad , \quad \text{at } x = x_1 \tag{17}$$

The same way, the conditions at $x = x_2$ are

$$\begin{aligned} u_2 - ew_2' &= u_3 & \qquad h_2 u_2' &= h_1 u_3' \\ w_2 &= w_3 & h_2^3 w_2'' + 12eh_2 u_2' &= h_1^3 w_3'' \\ w_2' &= w_3' & h_2^3 w_2''' &= h_1^3 w_3''' \end{aligned} \tag{18}$$

Remark 3. Boundary conditions (16) - (17) and (18) assure the energy conservation in the course of its transfer through the butt joints. This can make explicit, e.g., taking into account that in line with the conditions at $x = x_1$

$$A_1 u_1^{'} u_1^* = A_2 u_2^{'} u_2^* - A_2 e u_2^{'} (w_2^{'})^* \quad \text{and} \quad I_1 w_1^{''} (w_1^{'})^* = I_2 w_2^{''} u_2^* + A_2 e u_2^{'} (w_2^{'})^*.$$

The second terms with the eccentricity e are reduced in the sum of Eq. (11), hence, the expression for the amount of energy E_1 at the left of x_1 becomes the same as E_2 at the right side of the joint. Similarly for $x = x_2$.

4. REFLECTION AND TRANSMISSION COEFFICIENTS

The diffraction of an incident A_0 or S_0 wave by the notch gives rise to the reflected and transmitted fields $\mathbf{u}_1^-$ and $\mathbf{u}_3^+$. Thus the general solution of Eqs. (3), (4) in the whole domain $B = B_1 \cup B_2 \cup B_3$ may be represented in the following form

$$\begin{array}{ll} u_1 = u_0 + u_1^- = u_0 + c_1 e^{-i\zeta_1 (x - x_1)}, & x \in B_1 \\ u_2 = c_2 e^{i\zeta_1 (x - x_1)} + c_3 e^{-i\zeta_1 (x - x_2)}, & x \in B_2 \\ u_3 = u_3^+ = c_4 e^{i\zeta_1 (x - x_2)}, & x \in B_3 \end{array} \tag{19}$$

$$\begin{array}{ll} w_1 = w_0 + w_1^- = w_0 + c_5 e^{-i\zeta_{2,1} (x - x_1)} + c_6 e^{\zeta_{2,1} (x - x_1)}, & x \in B_1 \\ w_2 = c_7 e^{i\zeta_{2,2} (x - x_1)} + c_8 e^{-\zeta_{2,2} (x - x_1)} + c_9 e^{-i\zeta_{2,2} (x - x_2)} + c_{10} e^{\zeta_{2,2} (x - x_2)}, & x \in B_2 \\ w_3 = w_3^+ = c_{11} e^{i\zeta_{2,3} (x - x_2)} + c_{12} e^{-\zeta_{2,3} (x - x_2)}, & x \in B_3 \end{array} \tag{20}$$

The 12 unknown constants c_j, $j = 1, 2, ..., 12$, are obtained from the 12×12 system of linear equations resulting from the $6 + 6$ joining conditions (16) – (18).

The energy E^- and E^+ of the reflected and transmitted waves $\mathbf{u}^-$ and $\mathbf{u}^+$ may be obtained using the same formulas as Eqs. (12) but with the coefficients c_1 and c_5 substituted for A_0 and S_0 in the case of reflected wave energy $E^- = E_S^- + E_A^-$:

$$E_S^- = \frac{\omega}{2} Y A_1 \zeta_1 |c_1|^2, \quad E_A^- = \omega Y I_1 \zeta_{2,1}^3 |c_5|^2, \tag{21}$$

and with the amplitude constants c_4 and c_{11} for the transmitted wave energy $E^+ = E_S^+ + E_A^+$:

$$E_S^+ = \frac{\omega}{2} Y A_2 \zeta_1 |c_4|^2, \quad E_A^+ = \omega Y I_2 \zeta_{2,2}^3 |c_{11}|^2. \tag{22}$$

The values $E_S^\pm$ and $E_A^\pm$ are energy transferred by transmitted and reflected S_0 and A_0 GWs. With an ideally elastic waveguide structure, the energy balance is

$$\kappa^- + \kappa^+ = 1, \tag{23}$$

where the transmission and reflection coefficients $\kappa^\pm = E^\pm / E_0$ consist of specific coefficients for the scattered S_0 and A_0 waves:

$$\kappa^\pm = \kappa_S^\pm + \kappa_A^\pm = E_S^\pm / E_0 + E_A^\pm / E_0 \tag{24}$$

If only S_0 mode is taken as the incident field ($A_0 = 0$), the values $\kappa_S^\pm$ may be treated as the coefficients of its transmission and reflection ($\kappa_S^\pm \equiv \kappa_{SS}^\pm$), while $\kappa_A^\pm$ are the coefficients of its forward and backward conversion into A_0 modes ($\kappa_A^\pm \equiv \kappa_{SA}^\pm$). Similarly, with an A_0 incidence ($S_0 = 0$), $\kappa_A^\pm \equiv \kappa_{AA}^\pm$ and $\kappa_S^\pm \equiv \kappa_{AS}^\pm$.

5. 2D NOTCHED WAVEGUIDE

As a more complex model for GW diffraction by corrosion areas, a 2D notched elastic strip (Fig. 1b) governed by the full system of elastodynamic equations

$$(\lambda + 2\mu)\mathrm{div}\,\mathbf{u} + \mu\Delta\mathbf{u} + \rho\omega^2\mathbf{u} = 0 \tag{25}$$

has been also considered; λ and μ are Lamé constants of elasticity. In this statement, the coupling boundary conditions are different from those for the beams. They are the conditions of displacement and stress field continuity at the joint interface lines

$$[\mathbf{u}]_m = 0, \quad [\tau_x]_m = 0, \quad x = x_m, \quad -h_1/2 \le z \le h_1/2 - \Delta z, \quad m = 1,2 \tag{26}$$

and the stress-free conditions

$$\tau_x = 0, \quad x = x_m, \quad h_1/2 - \Delta z \le z \le h_1/2, \quad m = 1,2 \tag{27}$$

at the rest of edges of the thicker strips B_1 and B_3, not contacting with the thinner intermediate domain B_2. Square brackets denote here the jump of related vector functions at the cross-sections $x = x_m$. The horizontal sides of the notched domain are also stress-free.

The diffraction of an incident guided wave $\mathbf{u}_0(\mathbf{x}) = \mathbf{a}_0(z)e^{i\zeta_k x}$ gives rise to the scattered field $\mathbf{u}_{sc}(\mathbf{x})$, so that the total wave field in the notched waveguide is $\mathbf{u} = \mathbf{u}_0 + \mathbf{u}_{sc}$. Here ζ_k, $k = 1$ or 2, is the wavenumber of the fundamental S_0 or A_0 Lamb wave; these values tend to the beam's wavenumbers in Eqs. (3) – (4) as $\omega h\sqrt{\rho/Y} \to 0$; $\mathbf{a}_0(z)$ is an eigenform of the corresponding Lamb wave.

The scattered field is derived using the LEM technique [2] in the form

$$\mathbf{u}_{sc}(\mathbf{x}) = \int_S l(\mathbf{x},\xi)\mathbf{c}(\xi)d\xi, \tag{28}$$

where S is the boundary of the notch, $\mathbf{c}(\mathbf{x})$ is an unknown potential's density and $l(\mathbf{x},\xi) = [\mathbf{l}_1 \vdots \mathbf{l}_2 \vdots \mathbf{l}_3]$ is the matrix of fundamental solutions for the intact elastic layered structure under consideration. Its columns $\mathbf{l}_j$, $j = 1,2,3$, are displacements generated by the point sources $\delta(\mathbf{x}-\xi)\mathbf{i}_j$, where $\mathbf{i}_j$ are basic coordinate vectors. They satisfy the governing equations and the homogeneous boundary conditions at all plane-parallel surfaces (at the surfaces $z = \pm h_1/2$ in the case). A substitution of relation (28) into the boundary conditions on S yields a boundary integral equation with respect to the vector function $\mathbf{c}$. Its solution is obtained using boundary element method technique.

6. NUMERICAL EXAMPLES AND DISCUSSION

To estimate the range of practical applicability of the results obtained within the beam model, a systematic comparison of the transmission, reflection and conversion coefficients $\kappa^{\pm}$ obtained versus frequency within beam and LEM models have been carried out. Preliminary the LEM model has been validated against the known FEM and experimental results [5]. Figure 2 gives examples of such comparisons for the amplitude reflection coefficient $\mu^- = |w^-/w_0|$ of A_0 mode propagating in a steel plate of thickness $h_1 = 3$ mm. The left subplots show the frequency dependence of μ^- for two notches of width $\Delta x = h_1$ and depths $h_2 = 0.83h_1$ and $0.5h_1$. The right subplot illustrates the influence of the notch width Δx variation. The reflection coefficient μ^- is shown here versus the ratio $\Delta x/\lambda$, where $\lambda = 5.5$ mm is the A_0 wavelength at $f = 450$ kHz.

Figures 3 and 4 give examples of beam-to-LEM comparisons for two aluminium samples of thickness $h_1 = 1$ mm with the notches of length $\Delta x = 5$ mm and depths $\Delta z = 0.5$ and 0.75 mm ($h_2 = 0.5$ and 0.25 mm); the material properties $Y = 71$ GPa, $\rho = 2700$ kg/m^3 and Poisson's ratio $\nu = 1/3$. The figures are for S_0 and A_0 incidence. To avoid cluttering the figures, only transmission (blue)

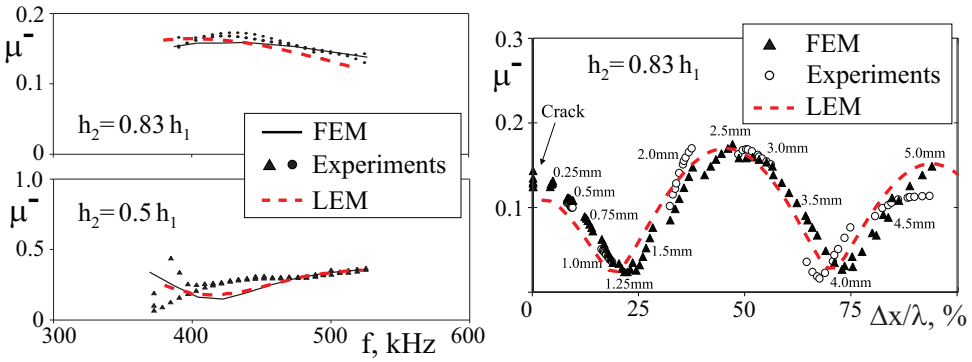

Figure 2 : Examples of LEM validation against FEM and experimental results [5].

and reflection (red) coefficients κ^+ and κ^- are shown without the coefficients of mode conversion, exhibiting similar rate of coincidence.

At relatively low frequencies $hf/v << 1$ (v is a characteristic wave velocity), the displacement field $\mathbf{u}$ in an elastic strip exhibits linear dependence on the cross coordinate z, as it is formulated in beam assumptions (1) - (2). The fundamental A_0 and S_0 Lamb waves are also well approximated by beam's guided waves (1), (2), (5) and (6).

On the other hand, linear behaviour of displacement and stress fields relative to z coordinate is violated near the lines of butt junction even in the limit $f \to 0$. Therefore, it is not clear how well the conditions of beam coupling may substitute for conditions (26) - (27). One more factor differing beam and strip models is that though the S_0 and A_0 modes of the latter become of form (1) - (2), (5) - (6) at low frequencies, their wavenumbers are slightly different from ζ_1 and ζ_2 diverging from them as frequency increases.

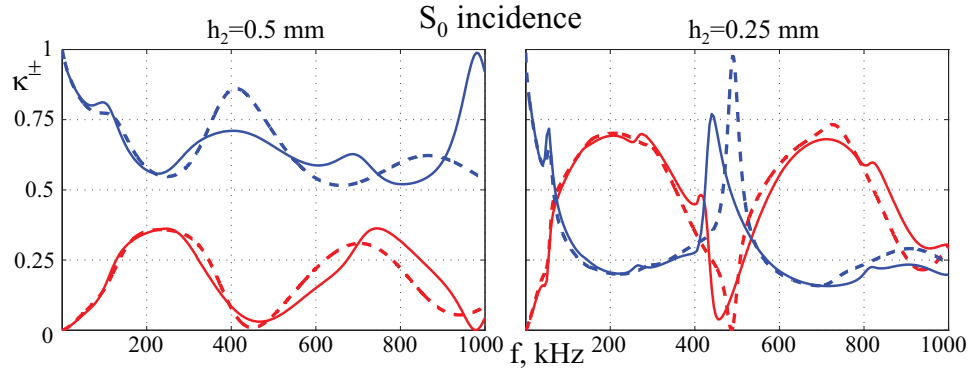

Figure 3 : Transmission (blue) and reflection (red) coefficients κ_S^+ and κ_S^- obtained within LEM and beam models (solid and dashed lines, respectively) for the S_0 mode in notched waveguides of web thicknesses $h_2 = 0.5$ and 0.25 mm; $h_1 = 1$ mm, $\Delta x = 5$ mm.

Nevertheless, the comparison of transmission and reflection coefficients $\kappa_S^\pm$ and $\kappa_A^\pm$ obtained for notched beams and strips has shown that at low frequencies the beam plots follow reasonably close to the strip counterparts (Figs. 3, 4). The coincidence of results for the S_0 incidence is visibly better then in the A_0 case. In the frequency range up to 300 kHz, it is very good. In the A_0 case the coincidence is not so good. Although, even with the most complicate curve behaviour at $h_2 = 0.25$ (Fig. 4, right), the beam curves catch the peaks and minima in the range $f \leq 100$ kHz, following them with a certain shift in a wider range as well.

One of the reasons for better beam model performance with S_0 incidence is the much better

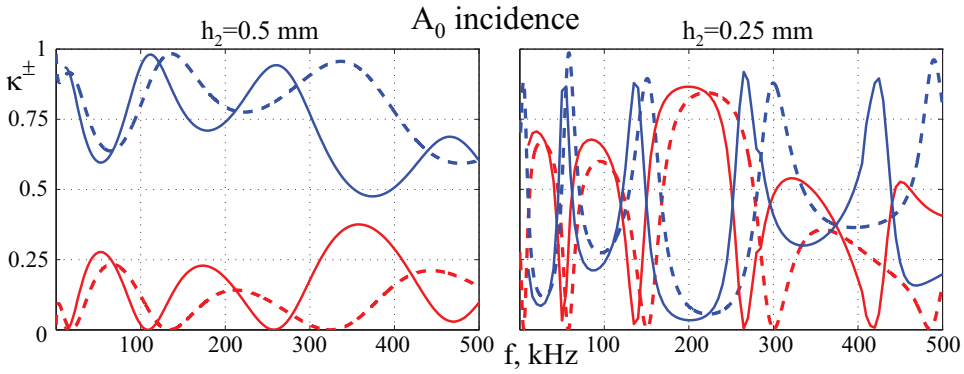

Figure 4 : Same as in Fig. 3 for A_0 incidence.

wavelength-to-thickness (λ/h) ratio than with A_0 waves. For example, at the frequencies $f = 100$ kHz and 500 kHz, these ratios for S_0 are $\lambda_S/h = 51.3$ and 10.3, while for A_0 they are $\lambda_A/h = 9.6$ and 2.9, respectively.

Conclusion

In spite of apparent simplicity of the Bernoulli-Euler beam equations, it is quite acceptable to use them for the simulation of GW diffraction by step and notch obstacles at low frequencies, at least in the first quarter of the two-mode Lamb wave range. The crucial point here is the formulation of coupling boundary conditions at eccentric butt joints. Only a proper accounting for the eccentricity provides the wave energy conservation across the junction as well as correct energy partition among the reflected and transmitted travelling waves.

The authors are grateful to Prof. W. Seemann, KIT, Karlsruhe, for the useful discussion of the beam model. The work is partly supported by the Russian Foundation for Basic Research (RFBR) (projects No. 12-01-00320 and 14-08-00370).

References

[1] E.D. Swenson, C.T. Owens, M.P. Desimio, and S.E. Olson. Comparisons of analytical and experimental measurements of lamb wave interaction with corrosion damage in aluminum plates. In *Proceedings of the 6th European Workshop on Structural Health Monitoring - EWSHM-2012*, number Fr.1.C.2, pages 1–8, 2012.

[2] Ye.V. Glushkov, N.V. Glushkova, A.A. Yeremin, and V.V. Mikhas'kiv. The layered element method in the dynamic theory of elasticity. *Journal of Applied Mathematics and Mechanics*, 73(4):449 – 456, 2009.

[3] E.V. Glushkov, N.V. Glushkova, and O.N. Lapina. Diffraction of normal modes in composite and stepped elastic waveguides. *Journal of Applied Mathematics and Mechanics*, 62(2):275–280, 1998.

[4] L. Moreau, M. Caleap, A. Velichko, and P.D. Wilcox. Scattering of guided waves by flat-bottomed cavities with irregular shapes. *Wave Motion*, 49(2):375 – 387, 2012.

[5] M. J. S. Lowe, P. Cawley, J-Y. Kao, and O. Diligent. The low frequency reflection characteristics of the fundamental antisymmetric lamb wave a_0 from a rectangular notch in a plate. *The Journal of the Acoustical Society of America*, 112(6):2612–2622, 2002.